J. Fluid Mech. (1970), *vol.* 43, *part* 3, *pp.* 607–635
Printed in Great Britain

An optical study of turbulence

By G. E. ROE

Department of Mechanical Engineering, Simon Engineering Laboratories, University of Manchester

(Received 7 August 1969 and in revised form 18 March 1970)

This paper describes theoretical and experimental work carried out at the Cavendish Laboratory of the University of Cambridge. The main object of the work was to develop a new technique for measuring the structure of fluid turbulence.

A parallel beam of light is passed through the turbulent region, containing refractive index fluctuations, and analyzed on exit by gratings of periodic transmissivity. Two forms of analysis yield (*a*) the spatial power spectrum of the refractive index fluctuations in the turbulence, and (*b*) the velocity distribution within the beam aperture. The method does not disturb the fluid physically, does not depend on the existence of a mean flow velocity, and works well in liquids.

One of the limitations of this single-beam method is that it produces information averaged along the path length of the beam in the turbulence, and to overcome this a cross-beam technique, using two beams intersecting at right-angles, has been developed in theory. This method gives the spatial power spectrum of the refractive index fluctuations, as does the single beam method, but the results are characteristic only of the volume of intersection of the beams.

The paper first discusses the theory of the single-beam and crossed-beam techniques, and then experimental results obtained with the single-beam method.

The turbulent region investigated was a rectangular tank of water, heated from below and cooled from above, producing convective turbulence of high Rayleigh number ($4{\cdot}1 \times 10^8$), a system difficult to analyze by conventional methods of measurement, such as the hot-wire anemometer.

Spectral density functions (power spectra) of refractive index, and hence in this case temperature fluctuations, have been measured, as have velocity distributions. Statistical analysis of the results also gives useful information about the Eulerian time scale of the turbulent field.

1. Introduction

When a wave motion is incident upon a field of turbulence, it is in general modified according to the structure of that field, and, on emerging, carries with it information about the field.

Much theoretical work has already been published on wave scattering by turbulence, but not for the purpose of developing new methods of measurement, rather to investigate problematic phenomena such as the propagation of radio

waves through the atmosphere, stellar scintillation, sound scattering in oceanography, and the problem of aircraft noise. Particular references are Batchelor (1957), Tatarski (1961) and Townsend (1965).

The hot-wire anemometer is probably the most important current method of measuring turbulent structure, but in many circumstances it has some inherent disadvantages, and optical methods are now receiving much attention as a possible alternative. The method proposed here has advantage over the hot wire principally because it (i) does not disturb the flow physically; (ii) works very well in liquids; (iii) gives meaningful results even when the mean flow velocity is zero, (iv) has a spatial resolution limit set by diffraction and beam divergence, which in practice is an improvement over the hot wire; (v) retains its calibration satisfactorily.

It naturally has limitations of its own, principally (i) the sampling volume (the volume of the beam in the turbulence) must be large compared with the scale of the turbulence being measured; (ii) the field must be reasonably homogeneous over this volume.

2. Theory of optical Fourier analysis by periodic grating

2.1. *The effect of a grating on a given incident intensity pattern*

For simplicity, a grating of square cross-section will be considered initially (figure 1).

Suppose the intensity falling on the grating is

$$I(\mathbf{r};t) = I_0 + \sum_{\mathbf{k}} a(\mathbf{k};z;t)e^{i\mathbf{k}.\mathbf{r}}, \tag{1}$$

i.e. a Fourier expansion in the x, y plane at z in wave-number $\mathbf{k} = (l, m)$; t = time, $\mathbf{r} = (x, y, z)$ and I_0 = constant.

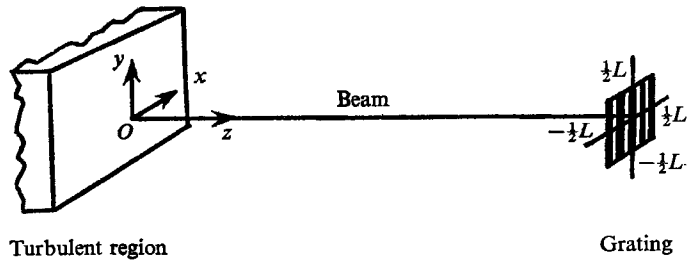

FIGURE 1. Basic geometry. All the light transmitted by the grating is focused onto a photocell.

Suppose also that the transmissivity of the grating is

$$T(x) = \beta(1 + \lambda \cos k_0 x). \tag{2}$$

Although in practice, it may be convenient to have a square-wave grating transmissivity, results so obtained can be corrected to those of a sinusoidal grating (see §2.6).

Thus the total amount of light transmitted by the grating, and received by the photocell, is (adding intensities, as appropriate when the period of the grating is large compared with the wavelength of light),

$$\begin{aligned} J(k_0;z;t) &= \int_{-\frac{1}{2}L}^{\frac{1}{2}L}\int_{-\frac{1}{2}L}^{\frac{1}{2}L} I(\mathbf{r};t)T(x)\,dx\,dy \\ &= \beta I_0 L^2 + I_0\beta\lambda\int_{-\frac{1}{2}L}^{\frac{1}{2}L}\int_{-\frac{1}{2}L}^{\frac{1}{2}L}\cos k_0 x\,dx\,dy \\ &\quad + \beta\int_{-\frac{1}{2}L}^{\frac{1}{2}L}\int_{-\frac{1}{2}L}^{\frac{1}{2}L}\sum_{\mathbf{k}} a(\mathbf{k};z;t)\,e^{i\mathbf{k}.\mathbf{r}}\,dx\,dy \\ &\quad + \tfrac{1}{2}\beta\lambda\int_{-\frac{1}{2}L}^{\frac{1}{2}L}\int_{-\frac{1}{2}L}^{\frac{1}{2}L}\sum_{\mathbf{k}} a(\mathbf{k};z;t)\,e^{i\mathbf{k}.\mathbf{r}}(e^{ik_0x}+e^{-ik_0x})\,dx\,dy. \end{aligned} \tag{3}$$

The first term in (3) is constant. If the grating has an integral number of periods, the second term is zero. If not, this term only contributes a small extra constant. Only fluctuating terms will ultimately be retained.

The third term is the integral of the fluctuations over the aperture with no grating present, $\times\beta$. If the aperture is sufficiently large, this term will be negligibly small. More rigorously,

$$\int_{-\frac{1}{2}L}^{\frac{1}{2}L}\int_{-\frac{1}{2}L}^{\frac{1}{2}L}\sum_{\mathbf{k}} a(\mathbf{k};z;t)\,e^{i\mathbf{k}.\mathbf{r}}\,dx\,dy = L^2\sum_{\mathbf{k}} a(\mathbf{k};z;t)\,\frac{\sin(\frac{1}{2}lL)}{\frac{1}{2}lL}\,\frac{\sin(\frac{1}{2}mL)}{\frac{1}{2}mL}.$$

Now the weighting functions $\sin(\frac{1}{2}lL)/\frac{1}{2}lL$, $\sin\frac{1}{2}mL/\frac{1}{2}mL$ peak at zero wavenumber, and have a half width $\sim \pi/L$. Also, $a(0;z;t) = 0$. Thus, if $a(\mathbf{k};z;t)$ does not attain large values for $l, m < \pi/L$, this is a small term. If not negligible, it represents a low-frequency background signal, independent of k_0, i.e. effectively a low-frequency noise output. It can be removed by using a high pass filter, or measured as $\beta^2\times$ (mean square signal with no grating present), with β typically $\lesssim \frac{1}{2}$. In the experimental results discussed later, this background was small compared with the noise level of the photocell.

Thus, from the last term of (3), the fluctuating part of the received light signal is, to a good approximation,

$$\Delta J(k_0;z;t) = \tfrac{1}{2}\beta\lambda L^2\sum_{\mathbf{k}} a(\mathbf{k};z;t)\,\frac{\sin(\frac{1}{2}mL)}{\frac{1}{2}mL}\,\frac{\sin[\frac{1}{2}(l-k_0)L]}{\frac{1}{2}(l-k_0)L}. \tag{4}$$

neglecting terms in $1/(l+k_0)$ compared with those in $1/(l-k_0)$ in the summation over $\mathbf{k} = (l, m)$. So, denoting complex conjugates by*,

$$\begin{aligned} \Delta J^2(k_0;z;t) = \tfrac{1}{4}\beta^2\lambda^2L^4\Bigg[&\sum_{\mathbf{k}} a(\mathbf{k};z;t)\,a^*(\mathbf{k};z;t)\left(\frac{\sin\frac{1}{2}mL}{\frac{1}{2}mL}\right)^2 \\ &\times\left\{\frac{\sin[\frac{1}{2}(l-k_0)L]}{\frac{1}{2}(l-k_0)L}\right\}^2 + \sum_{\substack{\mathbf{k}\\ \mathbf{k}\neq\mathbf{k}'}}\sum_{\mathbf{k}'} a(\mathbf{k};z;t)\,a^*(\mathbf{k}';z;t) \\ &\times\frac{\sin(\frac{1}{2}mL)}{\frac{1}{2}mL}\,\frac{\sin(\frac{1}{2}m'L)}{\frac{1}{2}m'L}\,\frac{\sin[\frac{1}{2}(l-k_0)L]}{\frac{1}{2}(l-k_0)L}\,\frac{\sin[\frac{1}{2}(l'-k_0)L]}{\frac{1}{2}(l'-k_0)L}\Bigg]. \end{aligned} \tag{5}$$

One now needs to assume some homogeneity in order to use the unrelated phase property of two wave-numbers. [For a homogeneous field, the phases of any two structure components corresponding to different wave-numbers are unrelated; see Batchelor (1959*a*).] Difficulty is experienced with Fourier sums for homogeneous fields, which are effectively infinite in spatial extent, and one must resort to Fourier–Stieltjes integrals or the simpler approach, used here, of assuming homogeneity over some dimension D, and assuming that the field has periodicity D. This enables Fourier series to be used.

Using $2\pi/k_0$ as typical of the scale of turbulence being measured, if $2\pi/k_0 \ll D$, the unrelated phase property can be used as an approximation, reducing to negligible size the double sum of equation (5), in time average.

The component wave-numbers in (1) are integral multiples of $2\pi/D$. Also, the width of the weighting functions of type $\sin(\frac{1}{2}mL)/\frac{1}{2}mL$ is of order $2\pi/L$, so if $D \gg L$, the remaining sum in (5) can be replaced by an integral, and if $2\pi/L \ll k_0$, $a(\mathbf{k}; z; t)$ can be replaced by its value at the central wave-number of the weighting functions, i.e. $\mathbf{k} = (k_0, 0)$.

Making these approximations, the time average of (5) becomes

$$\overline{\Delta J^2(k_0; z)} = \pi^2\beta^2\lambda^2L^2(D/2\pi)^2\,\overline{a(k_0, 0; z; t)\,a^*(k_0, 0; z; t)} \tag{6}$$

subject to the conditions $\qquad D \gg L, \quad k_0L \gg 2\pi. \tag{7}$

The grating therefore acts as a spatial filter for the wave-number $(k_0, 0)$. Gratings have been used by Protheroe (1964) to analyze stellar shadow bands.

2.2. *The spectral density function, or 'power spectrum'*

For a given function $f(\mathbf{r}; t)$, the corresponding spectral density function, $F(\mathbf{K})$, can be defined as the contribution to $\overline{f^2(\mathbf{r}; t)}$ per unit volume of $\mathbf{K}$ space, at wave-number $\mathbf{K} = (l, m, n)$, so

$$\overline{f^2(\mathbf{r}; t)} = \iiint_{\text{all } \mathbf{K} \text{ space}} F(\mathbf{K})\,d\mathbf{K}. \tag{8}$$

Also, for a homogeneous field, $F(\mathbf{K})$ can be defined as the Fourier transform of the correlation function formed from $f(\mathbf{r}; t)$ at two points $\mathbf{r}_1$, $\mathbf{r}_2$, viz.

$$\overline{f(\mathbf{r}_1; t)f(\mathbf{r}_2; t)} = \iiint F(\mathbf{K})\,e^{i\mathbf{K}.(\mathbf{r}_1-\mathbf{r}_2)}\,d\mathbf{K}. \tag{9}$$

Equation (8) then follows from (9) with $\mathbf{r}_1 = \mathbf{r}_2$. $F(\mathbf{K})$ is thus of fundamental importance in turbulence theory.

If $f(\mathbf{r}; t)$ is written as a Fourier sum

$$f(\mathbf{r}; t) = \sum_{\mathbf{K}} q(\mathbf{K}; t)\,e^{i\mathbf{K}.\mathbf{r}}, \tag{10}$$

then $$F(\mathbf{K}) = (D/2\pi)^3\,\overline{q(\mathbf{K}; t)\,q^*(\mathbf{K}; t)} \tag{11}$$

using the unrelated phase property as in § 2.1.

One form for $f(\mathbf{r}; t)$ which will be used later is

$$f(\mathbf{r}; t) = \sum_{\mathbf{K}} Q(\mathbf{K}; t)\cos[\mathbf{K}.\mathbf{r} + \alpha(\mathbf{K}; t)] \tag{12}$$

with Q, α real. In this case (Roe 1968),

$$F(\mathbf{K}) = \tfrac{1}{2}(D/2\pi)^3 \overline{Q^2(\mathbf{K};t)}. \tag{13}$$

In two dimensions, $\mathbf{K} = (l, m, n)$ becomes $\mathbf{k} = (l, m)$ and the $(D/2\pi)^3$ factors become $(D/2\pi)^2$.

It is now clear, from (6) and (11), that the mean-square fluctuation in the light signal, $\overline{\Delta J^2(k_0; z)}$, is proportional to one component of the spectral density function of the intensity fluctuations incident upon the grating (the $(k_0, 0)$ component).

Hereafter, 'spectral density function' will be abbreviated to 's.d.f.'

2.3. *The relation between the s.d.f. of intensity fluctuations incident on the grating and the s.d.f. of refractive index fluctuations in the turbulent region*

Assume that wave amplitudes of light scattered from the turbulence are small compared with that of the incident beam (a valid assumption in practice). A suitable optical arrangement providing a parallel beam through the turbulence is shown in figure 2.

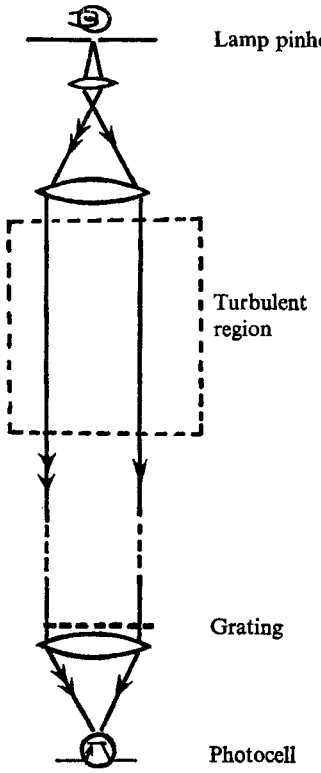

FIGURE 2. A suitable optical arrangement.

Let a monochromatic plane wave pass through a thin layer having refractive index variations in space and time. The wave emerges with an amplitude little different from the incident amplitude, but with phase variations in the x, y plane (the beam is taken as the z axis).

Let the incident wave be $\exp[i(Nz-\omega t)]$, where $N = 2\pi/$(light wavelength in medium outside turbulent region), ω = angular frequency. The time variation will be assumed implicitly hereafter.

If $z = 0$ is the exit plane from the layer, the complex amplitude at this plane, relative to that for no refractive index variations, will be

$$\exp[i\phi(x,y)], \quad \text{where} \quad \phi = N\int_{-h}^{0}(\mu-\mu_0)dz, \tag{14}$$

$\mu(\mathbf{r};t)$ = local refractive index, μ_0 = mean refractive index and h = layer thickness.

When $\phi \ll 1$ (thin layer),

$$\exp[i\phi(x,y)] = 1+i\sum_{\mathbf{k}} b(\mathbf{k})\cos[\mathbf{k}.\mathbf{r}+\alpha(\mathbf{k})], \tag{15}$$

where ϕ has been written as a Fourier sum over wave-number $\mathbf{k} = (l,m)$. $b(\mathbf{k})$ and $\alpha(\mathbf{k})$ are real functions of $\mathbf{k}$, and time. The cosine form is used here to avoid confusion of exponentials in the sum with $e^{i\phi}$.

The s.d.f. of phase fluctuations is thus, from (13) and (15),

$$\Phi(k) = \tfrac{1}{2}(D/2\pi)^2\overline{b^2(\mathbf{k})}. \tag{16}$$

The first term in (15) corresponds to the original incident wave, and the second to a summation over wave-number of a pair of scattered waves

$$\tfrac{1}{2}b(\mathbf{k})\exp[i(lx+my+n'z+\alpha)]+\tfrac{1}{2}b(\mathbf{k})\exp[-i(lx+my-n'z+\alpha)],$$

with wave normals in directions (l,m,n') and $(-l,-m,n')$ respectively, the light wave-number changing, on passing through the turbulence, from (O,O,N) to (l,m,n'). By conservation of vector wave-number,

$$l^2+m^2+n'^2 = N^2. \tag{17}$$

For planes other than $z = 0$, the z dependence can now be introduced, remembering that the incident wave is e^{iNz}. The total incident + scattered wave is thus, from (15),

$$\exp[iNz]+i\sum_{\mathbf{k}}\exp[in'z]b(\mathbf{k})\cos(\mathbf{k}.\mathbf{r}+\alpha)$$
$$= \exp[iNz][1+i\sum_{\mathbf{k}}\exp[i(n'-N)z]b(\mathbf{k})\cos(\mathbf{k}.\mathbf{r}+\alpha)]. \tag{18}$$

Multiplying this by its complex conjugate, to the same approximation of weak scattering, intensity variations are given by

$$I(\mathbf{r}) = I_0+2I_0\sum_{\mathbf{k}}\sin[(N-n')z]b(\mathbf{k})\cos(\mathbf{k}.\mathbf{r}+\alpha), \tag{19}$$

where unit incident intensity is now replaced by I_0. It is this intensity pattern $I(\mathbf{r})$ which falls on the grating, at z. Compare (19) with (1).

The s.d.f. of the intensity fluctuations is, from (1), (11), (13) and (19),

$$(D/2\pi)^2\overline{a(\mathbf{k};z)a^*(\mathbf{k};z)} = \tfrac{1}{2}(D/2\pi)^2 4I_0^2\sin^2[(N-n')]z\overline{b^2(\mathbf{k})}$$
$$= 4I_0^2\sin^2[(N-n')z].\Phi(\mathbf{k}) \tag{20}$$

using (16).

The largest wave-numbers of phase variation are much smaller than the optical wave-number N, so $l^2+m^2 \ll N^2$, and, from (17) we may write

$$N-n' = (l^2+m^2)/2N. \tag{21}$$

Let us now express the refractive index fluctuations in the turbulent region as a Fourier sum, i.e. write

$$\mu-\mu_0 = \sum_{\mathbf{K}} g(\mathbf{K})\cos[\mathbf{K}.\mathbf{r}+\gamma(\mathbf{K})], \tag{22}$$

where $\mathbf{K} = (l, m, n)$ as before, $g(\mathbf{K})$ and $\gamma(\mathbf{K})$ are real functions of $\mathbf{K}$, and time.

The s.d.f. of $\mu-\mu_0$ is thus, from (12) and (22),

$$G(\mathbf{K}) = \tfrac{1}{2}(D/2\pi)^3\overline{g^2(\mathbf{K})}. \tag{23}$$

One can then readily show, from (14), (22) and (23), the following relation between power spectra,

$$\Phi(\mathbf{k}) = (D/2\pi)^{-1}4N^2\sum_n \frac{G(\mathbf{K})}{n^2}\sin^2(\tfrac{1}{2}nh), \tag{24}$$

in which the summation can be replaced by an integral if $D \gg h$.

Thus, from (20) and (24), with the approximation (21),

$$(D/2\pi)^2\overline{a(\mathbf{k};z)a^*(\mathbf{k};z)} = 8I_0^2\sin^2\left[\frac{(l^2+m^2)z}{2N}\right]N^2h\int_{-\infty}^{\infty} G(\mathbf{K})\frac{\sin^2(\frac{1}{2}nh)}{(\frac{1}{2}nh)^2}\,d(\tfrac{1}{2}nh). \tag{25}$$

If $nh \gg 2\pi$ or $k_0h \gg 2\pi$, using k_0 as the measured wave-number scale, $G(\mathbf{K})$ will not vary substantially from its value at the centre of the weighting function (at $n = 0$) for significant contributions to the integral, so approximately

$$(D/2\pi)^2\overline{a(\mathbf{k};z)a^*(\mathbf{k};z)} = 8I_0^2\sin^2\left[\frac{(l^2+m^2)z}{2N}\right]N^2h\pi G(l,m,0), \tag{26}$$

subject to the conditions $\quad D \gg h \quad$ and $\quad k_0h \gg 2\pi.$ (27)

A result similar to (26) has been proved by Townsend (1965) and Tatarski (1961).

2.4. *The relation between the measured light signal and the s.d.f. of the refractive index fluctuations in the turbulent region*

From (6) and (26), the time mean-square fluctuation in the light signal received by the photocell is,

$$\overline{\Delta J^2(k_0;z)} = 8\pi^3I_0^2\beta^2\lambda^2L^2N^2h\sin^2(k_0^2z/2N)\,G(k_0,0,0), \tag{28}$$

subject to $\qquad D \gg h, L; \quad k_0h \gg 2\pi; \quad k_0L \gg 2\pi.$ (29)

Summarizing these conditions, therefore, the grating must have many lines within its width L, the sampling volume $(L\times L\times h)$ must be large compared with the scale of turbulence being measured, and the field must be homogeneous over at least the sampling volume. The latter condition need not be applied too strictly if mean values over the sampling volume are required.

From (28), note the following;

(i) It is $G(k_0, 0, 0)$ which one hopes to measure here, by varying k_0, i.e. by using a succession of gratings. Turning the grating through 90° measures $G(0, k_0, 0)$.

(ii) For small $k_0^2 z/2N$, sensitivity is increased by increasing z, until limited by beam divergence and aperture diffraction (Roe 1968).

(iii) For small $k_0^2 z/2N$, the mean square signal fluctuations $\propto k_0^4 G$. If a sufficiently wide equilibrium range of wave-numbers exist, there is theoretical support for $G \propto k_0^{-p}$, where p is approximately 4 (see §7.3). Thus the above light signal has a weak dependence on k_0, and detection apparatus need only cover a small range of signal strength. This is most convenient when measuring strong power-law variations of this kind.

(iv) The mean-square signal fluctuation $\propto$ area of grating (L^2), and not the square of this. This is because increasing the grating dimension L increases the transmission area as L^2, but the weighting function in (5) varies its width as L^{-1}.

(v) The mean square signal fluctuation $\propto h$, and not to h^2. This is due to the 'random walk' nature of the beam path through the turbulence.

(vi) The method is particularly useful in measuring a one-dimensional spectrum in the strict sense, i.e. $G(l, m, n)$ with any two of l, m, n zero (the full K space distribution is obtained by varying the beam direction, if desired). It does not measure a summation of all distributions with a component in the chosen direction (as does a hot wire with velocity distributions); neither does it average G over all directions. The extent of anisotropy can thus be found. Note that

$$\overline{(\mu-\mu_0)^2} = \int\int\int G(l,m,n)\,d\mathbf{K} = \int 4\pi K^2 G(K)\,dK \qquad (30)$$

in the isotropic case, with $K = (l^2+m^2+n^2)^{\frac{1}{2}}$.

In thermal turbulence, where the refractive index field is due to temperature variation, the s.d.f. of refractive index fluctuations is proportional to the s.d.f. for density and temperature fluctuations, for small fluctuations of temperature.

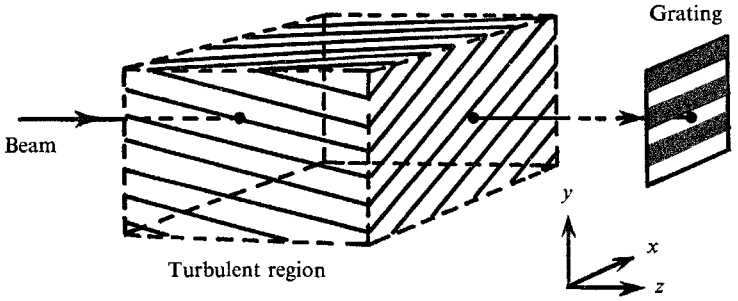

FIGURE 3. Diagrammatic representation of optical Fourier analysis.

(vii) A simple illustration of this method is shown in figure 3, where the inclined lines represent wave crests (or troughs) in the spatial variation of some arbitrary Fourier component. Both along the path of the beam, and along the lines of the grating, the crests and troughs tend to average out, giving a zero light signal fluctuation. Only when $l = n = 0$, and the crests and troughs are parallel to the plane defined by the beam direction and grating lines, does the grating transmit a signal fluctuation, corresponding in this case to $G(0, k_0, 0)$.

2.5. *Removal of the assumption that the scattering thickness should be small*

If the scattering thickness (length of beam path through turbulent region), H, is considerably greater than the scale of the turbulence, the pattern at the grating, and hence the measured light signal is a superposition of independent contributions from thin layers at all distances from z to $z+H$.

Therefore from (28), replacing h by dz, and integrating from z to $z+H$,

$$\overline{\Delta J^2(k_0;z)} = 4\pi^3 I_0^2 \beta^2 \lambda^2 L^2 N^3 E(k_0^2/N, z, H) G(k_0, 0, 0), \tag{31}$$

where

$$E(k_0^2/N, z, H) = (1/k_0^2)\,[k_0^2 H/N + 2\cos[k_0^2(z+\tfrac{1}{2}H)/N]\sin(k_0^2 H/2N)]. \tag{32}$$

This function E can be calculated for a given experimental configuration, as a function of k_0. Note that as $k_0 \to 0$,

$$E \to (H/2N^3)\,(z+\tfrac{1}{2}H)^2 k_0^4 \quad \text{and} \quad \overline{\Delta J^2(k_0;z)}$$

$$\to 2\pi^3 I_0'^2 \beta^2 \lambda^2 L^2 H (z+\tfrac{1}{2}H)^2 k_0^4 G(k_0, 0, 0). \tag{33}$$

This is independent of N, the wave-number of the light used. Thus if E is calculated from (32) and found to be a good approximation to a fourth power dependence on k_0 over the range of k_0 used, the dependence of $\overline{\Delta J^2}$ on N will be small, enabling white, instead of monochromatic light to be used.

2.6. *Harmonic correction for a square wave grating*

The theory of §2.1 assumes a grating of transmissivity

$$T(x) = \beta(1+\lambda\cos k_0 x) \simeq \beta(1+\cos k_0 x) \tag{34}$$

in practice.

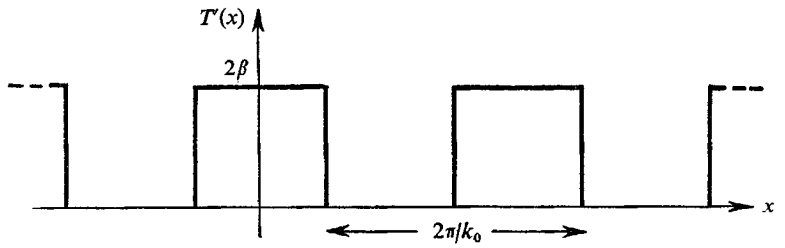

FIGURE 4. Square wave grating transmissivity.

The simplest grating to manufacture photographically (and that used in the present experimental arrangement) has the periodic transmissivity $T'(x)$ shown in figure 4, which can be written

$$T'(x) = \beta[1 + (4/\pi)\,(\cos k_0 x - \tfrac{1}{3}\cos 3k_0 x + \tfrac{1}{5}\cos 5k_0 x - \ldots)]. \tag{35}$$

Using (35), instead of (2), in (3) produces the square wave grating mean-square light-signal fluctuation, written here as $\overline{\Delta J_s^2}$, of

$$\overline{\Delta J_s^2(k_0;z)} = (16/\pi^2)\,[\overline{\Delta J^2(k_0;z)} + \tfrac{1}{9}\overline{\Delta J^2(3k_0;z)} + \tfrac{1}{25}\overline{\Delta J^2(5k_0;z)} + \ldots], \tag{36}$$

where $\overline{\Delta J^2}$ is the mean-square light-signal fluctuation for an equivalent sinusoidal grating.

Writing similar relations for $\overline{\Delta J_s^2(3k_0;z)}$, $\overline{\Delta J_s^2(5k_0;z)}$, etc., one has a set of simultaneous linear equations which can be written in matrix form and solved to give

$$\overline{\Delta J^2(k_0;z)} = (\pi^2/16)\,[\overline{\Delta J_s^2(k_0;z)} - \tfrac{1}{9}\overline{\Delta J_s^2(3k_0;z)} - \tfrac{1}{25}\overline{\Delta J_s^2(5k_0;z)}\ldots]. \tag{37}$$

The square wave grating gives a plot of $\overline{\Delta J_s^2}$ *vs.* k_0. This can then be corrected to a plot of $\overline{\Delta J^2}$ *vs.* k_0 (as required) using (37).

2.7. *The case of a circular aperture*

The theory so far presented has been for a square beam aperture of side L. It may be more convenient in practice to have a circular aperture, of radius R, say. Equation (4) then becomes

$$\Delta J(k_0;z;t) = \pi\beta\lambda R^2 \sum_{\mathbf{k}} a(\mathbf{k};z;t)\,\frac{J_1(k_- R)}{(k_- R)}, \tag{38}$$

where $(k_-)^2 = (l-k_0)^2 + m^2$, and J_1 is the Bessel function of order unity.

The weighting function

$$L^2[\sin(\tfrac{1}{2}mL)/\tfrac{1}{2}mL]\,[\sin[\tfrac{1}{2}(l-k_0)L]/\tfrac{1}{2}(l-k_0)L]$$

has become $$2\pi R^2 J_1(k_- R)/(k_- R).$$

As $(l,m)\to(k_0,0)$, both these functions tend to the area of the grating, L^2 and πR^2 respectively. Likewise, one can show that the only change in the fundamental result (28) is a substitution of πR^2 for L^2, viz.

$$\overline{\Delta J^2(k_0;z)} = 8\pi^4 I_0^2 \beta^2 \lambda^2 R^2 N^2 h \sin^2(k_0^2 z/2N)\,G(k_0,0,0). \tag{39}$$

The validity conditions (29) become

$$D \gg h, R; \quad k_0 h \gg 2\pi; \quad k_0 R \gg 4. \tag{40}$$

3. The use of crossed beams

3.1. *The need for crossed beams*

One of the main objections to the single-beam method discussed so far is that the measured information is the integrated effect over the path length of the beam through the turbulence. In cases of reasonable homogeneity, this is of little matter, but there is generally a need to obtain information characteristic of a certain sample of the total turbulent volume.

This can be achieved in the present case by having two beams intersecting at right-angles, when it can be shown that the information received is characteristic only of the volume of intersection of the beams. Unlike the single-beam case, this has not been tested experimentally. The following discussion is therefore proposal only.

The case of two crossed beams which suffer absorption only has been considered by Fisher & Krause (1967), and they have obtained results which compare favourably with established hot-wire results.

3.2. *Theory of the crossed-beam method*

For the sake of brevity, references will be made, where possible, to the single-beam theory of § 2, and a slightly different order of argument will be used (the previous order emphasized the relations between the various power spectra).

It will be assumed initially that signal contributions come from a path length $L_{1,2}$ rather greater than h (see figure 5), and then shown that only the length h is in fact relevant.

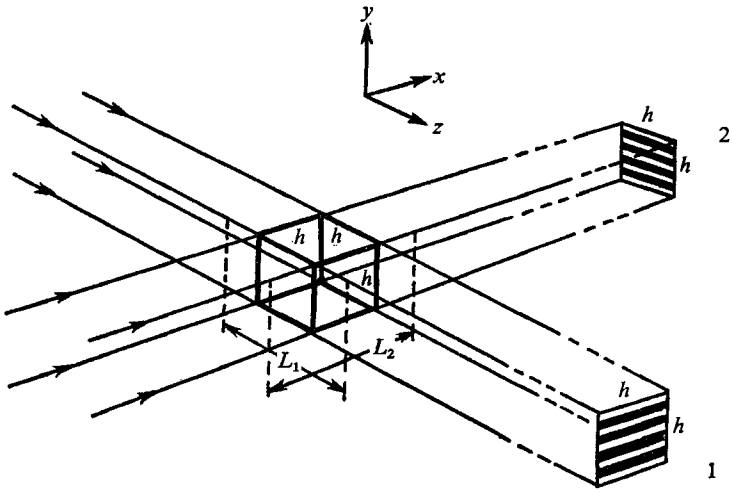

FIGURE 5. The crossed-beam technique.

The refractive index field will again be written as the Fourier sum of equation (22).

For beam 1, the relative phase shift on travelling a length L_1 of fluid (including the length h), taking $z = 0$ as the exit plane, is therefore, as in (14),

$$\begin{aligned}\phi(x,y) &= N\int_{-L_1}^{0}(\mu-\mu_0)\,dz \\ &= NL_1\sum_{\mathbf{K}} g(\mathbf{K})\,\frac{\sin(\frac{1}{2}nL_1)}{\frac{1}{2}nL_1}\cos(lx-my+\gamma-\tfrac{1}{2}nL_1). \qquad (41)\end{aligned}$$

The complex amplitude at this plane will be (for unit incident amplitude) $\exp[i\phi] \doteq 1+i\phi$ for small angles of scattering. For other values of z, taking the incident wave as $\exp[iNz]$, time variation being assumed implicitly, the total amplitude is therefore

$$\exp[iNz]\left[1+iNL_1\sum_{\mathbf{K}}\exp\left[-i\,\frac{(l^2+m^2)}{2N}\,z\right]g(\mathbf{K})\,\frac{\sin(\frac{1}{2}nL_1)}{\frac{1}{2}nL_1}\cos(lx+my+\gamma-\tfrac{1}{2}nL_1)\right]$$

using (21). (42)

Intensity variations are obtained by multiplying (42) by its complex conjugate (to the approximation of weak scattering used throughout), and for incident intensity I_0, the fluctuations falling on grating 1, at $z = d_1$, are

$$\Delta I_1(x,y) = 2I_0NL_1\sum\sin\left[\frac{(l^2+m^2)}{2N}d_1\right]g(\mathbf{K})\,\frac{\sin(\frac{1}{2}nL_1)}{\frac{1}{2}nL_1}\cos(lx+my+\gamma-\tfrac{1}{2}nL_1). \qquad (43)$$

The intensity fluctuations transmitted by grating 1, with transmissivity $\beta(1+\lambda\cos k_0 y)$, are

$$\Delta J_1 = \int_{-\frac{1}{2}h}^{\frac{1}{2}h}\int_{-\frac{1}{2}h}^{\frac{1}{2}h} \Delta I_1(x,y)\beta(1+\lambda\cos k_0 y)\,dx\,dy, \tag{44}$$

which gives, neglecting the constant background signal as before,

$$\Delta J_1 = \beta\lambda N L_1 h^2 I_0 \sum_{\mathbf{K}} \sin\left[\frac{l^2+m^2}{2N}d_1\right] g(\mathbf{K})\cos(\gamma-\tfrac{1}{2}NL_1) \times \frac{\sin(\frac{1}{2}nL_1)}{\frac{1}{2}nL_1}\frac{\sin(\frac{1}{2}lh)}{\frac{1}{2}lh}\frac{\sin[\frac{1}{2}(m-k_0)h]}{\frac{1}{2}(m-k_0)h}. \tag{45}$$

Similarly, the intensity fluctuations transmitted by grating 2 are,

$$\Delta J_2 = \beta\lambda N L_2 h^2 I_0 \sum_{\mathbf{K}} \sin\left[\frac{m^2+n^2}{2N}d_2\right] g(\mathbf{K})\cos(\gamma-\tfrac{1}{2}lL_2) \times \frac{\sin(\frac{1}{2}lL_2)}{\frac{1}{2}lL_2}\frac{\sin(\frac{1}{2}nh)}{\frac{1}{2}nh}\frac{\sin[\frac{1}{2}(m-k_0)h]}{\frac{1}{2}(m-k_0)h}. \tag{46}$$

$g(\mathbf{K})$ and γ are the same as in (45), for although the path length from volume of intersection to grating may be different in the two cases, information travels at the speed of light. For simplicity, the two gratings have been assumed identical.

The correlation between the two signals is thus

$$\overline{\Delta J_1 \Delta J_2} = \beta^2\lambda^2 N^2 L_1 L_2 h^4 I_0^2 \sum_{\mathbf{K}} \overline{g^2(\mathbf{K})}\cos(\gamma-\tfrac{1}{2}nL_1)\cos(\gamma-\tfrac{1}{2}lL_2) \times \frac{\sin(\frac{1}{2}nL_1)}{\frac{1}{2}nL_1}\frac{\sin(\frac{1}{2}nh)}{\frac{1}{2}nh}\frac{\sin(\frac{1}{2}lL_2)}{\frac{1}{2}lL_2}\frac{\sin(\frac{1}{2}lh)}{\frac{1}{2}lh}\frac{\sin^2[\frac{1}{2}(m-k_0)h]}{[\frac{1}{2}(m-k_0)h]^2} \times \sin\left[\frac{l^2+m^2}{2N}d_1\right]\sin\left[\frac{m^2+n^2}{2N}d_2\right]. \tag{47}$$

Terms of type $\overline{g(\mathbf{K}_1)g(\mathbf{K}_2)}$ are zero, approximately, in a reasonably homogeneous field, i.e. when $k_0 D \gg 2\pi$, as in the single-beam case, for then there is little correlation between different wave-number components.

Now if the widths of the weighting functions in (47) are small compared with the magnitude of the central wave-number, the various functions of (l,m,n) can be replaced approximately by their values at this central wave-number, namely at $(0,k_0,0)$. This condition is equivalent to $k_0 h \gg 2\pi$, since $L_{1,2} > h$. Therefore

$$\overline{\Delta J_1 \Delta J_2} = \beta^2\lambda^2 N^2 L_1 L_2 h^4 I_0^2 \sin\left(\frac{k_0^2 d_1}{2N}\right)\sin\left(\frac{k_0^2 d_2}{2N}\right) G(0,k_0,0) \times \int_{-\infty}^{\infty}\frac{\sin(\frac{1}{2}nL_1)}{\frac{1}{2}nL_1}\frac{\sin(\frac{1}{2}nh)}{\frac{1}{2}nh}\,dn \times \int_{-\infty}^{\infty}\frac{\sin(\frac{1}{2}lL_2)}{\frac{1}{2}lL_2}\frac{\sin(\frac{1}{2}lh)}{\frac{1}{2}lh}\,dl \int_{-\infty}^{\infty}\frac{\sin^2[\frac{1}{2}(m-k_0)h]}{[\frac{1}{2}(m-k_0)h]^2}\,dm. \tag{48}$$

Here, (23) has been used, and the sums written as integrals under the condition $D \gg h$.

From standard tables, the last integral is $2\pi/h$. The other two integrals are of the same type, and by writing the function $(\sin p)/p$ as the Fourier transform of a 'top-hat' function, one can show that

$$\int_{-\infty}^{\infty} \frac{\sin(\frac{1}{2}qL_{1,2})}{\frac{1}{2}qL_{1,2}} \frac{\sin(\frac{1}{2}qh)}{\frac{1}{2}qh}\, dq = 2\pi/L_{1,2}. \tag{49}$$

Using these integral results, (48) becomes

$$\overline{\Delta J_1 \Delta J_2} = 8\pi^3 I_0^2 \beta^2 \lambda^2(h^2) N^2 h \sin\left(\frac{k_0^2 d_1}{2N}\right) \sin\left(\frac{k_0^2 d_2}{2N}\right) G(0, k_0, 0). \tag{50}$$

Compare this with the single-beam result (28)

$$\overline{\Delta J^2} = 8\pi^3 I_0^2 \beta^2 \lambda^2(L^2) N^2 h \sin^2(k_0^2 d/2N) G(0, k_0, 0).$$

If one remembers that the grating area in (28) is L^2, and in (50) is h^2, this is a notable result, for if we put $d_1 = d_2 = d$, then $\overline{\Delta J_1 \Delta J_2}$ is equal to $\overline{\Delta J^2}$, with one important qualification; $G(0, k_0, 0)$ is averaged over the beam length in (28), but it is the mean value only over the volume of intersection of the beams in (50), this equation being independent of L_1 and L_2 and depending only on a scattering thickness h.

The assumptions made in this derivation are exactly analogous to the single-beam case, and can be reduced to the statements: (i) many lines are needed in each grating, i.e. the sampling volume must be large compared with the structure being measured; (ii) homogeneity is needed over a scale at least that of the sampling volume.

Note that the method measures the one-dimensional spectrum component in the direction normal to the plane containing the beams.

4. The determination of velocity distributions

4.1. *The principle*

The use of grating analysis of a light beam, so far described for determining structure power spectra, can be extended to measure velocity distributions.

Basically, one regards the intensity pattern incident upon the grating as moving rigidly past it. The frequency distribution of the output light signal is then characteristic of the velocity distribution within the aperture (in the direction normal to the lines of the grating) and of the periodicity of the grating used. As presented here, this is for the single-beam case only.

4.2. *The theory*

Let the direct signal from the photo-cell be $f(t)$, where t = time, and consider it sampled for a time T. $f(t)$ is fed to one input of a multiplier unit. Write $f(t)$ as a Fourier sum in which the component frequencies are integral multiples of $2\pi/T$, i.e.

$$f(t) = \sum_{\omega=-\infty}^{\infty} F(\omega)\, e^{i\omega t}, \tag{51}$$

where, from (8) and (11)

$$\overline{f^2(t)} = (T/2\pi) \int_{-\infty}^{\infty} F(\omega) F^*(\omega)\, d\omega. \tag{52}$$

The other input of the multiplier (response constant j) is fed with a signal $a\cos\omega_0 t$, giving the product signal

$$jf(t)\,a\cos\omega_0 t = ja\sum_{\omega}[\tfrac{1}{2}F(\omega)\,e^{i(\omega+\omega_0)t}+\tfrac{1}{2}F(\omega)\,e^{i(\omega-\omega_0)t}]$$

$$= ja\sum_{\omega'}\tfrac{1}{2}F(\omega'-\omega_0)\,e^{i\omega' t}+ja\sum_{\omega''}\tfrac{1}{2}F(\omega''+\omega_0)\,e^{i\omega'' t}. \tag{53}$$

Since $f(t)$ is a stationary random function, so is $jf(t)a\cos\omega_0 t$, and its s.d.f. can be written, using (11), as

$$\mathscr{F}(\omega) = j^2a^2[(T/2\pi)\tfrac{1}{4}F(\omega-\omega_0)F^*(\omega-\omega_0)+(T/2\pi)\tfrac{1}{4}F(\omega+\omega_0)F^*(\omega+\omega_0)]. \tag{54}$$

This assumes no correlation between the phases of different frequency components, i.e. $T \gg$ time scale of $f(t)$.

The product signal is then passed through a low-pass filter, which effectively has a band width $\Delta\omega$ on each side of zero frequency. The mean square output from the filter is then

$$S = \int_{-\Delta\omega}^{\Delta\omega}\mathscr{F}(\omega)\,d\omega, \tag{55}$$

the integral over a discrete frequency range being valid if $T\Delta\omega \gg 2\pi$. Therefore

$$S = j^2\tfrac{1}{2}a^2(T/2\pi)\cdot\frac{1}{2}\left[\int_{-\Delta\omega-\omega_0}^{\Delta\omega-\omega_0}FF^*(\omega)\,d\omega+\int_{-\Delta\omega+\omega_0}^{\Delta\omega+\omega_0}FF^*(\omega)\,d\omega\right]$$

$$= j^2\tfrac{1}{2}a^2(T/2\pi)\,(2\Delta\omega)\tfrac{1}{2}[FF^*(-\omega_0)+FF^*(\omega_0)], \tag{56}$$

since $\omega_0 \gg \Delta\omega$ for a filter of very narrow pass band.

The mean-square filter output is thus $j^2\times$(mean square input oscillation) $\times$(total bandwidth of filter) $\times$(even part of power spectrum of f, evaluated at input oscillation frequency ω_0.)

It is convenient to write the even part of the power spectrum of $f(t)$ as $M(\omega)$, so

$$S(\omega_0) = j^2\tfrac{1}{2}a^2(2\Delta\omega)\,M(\omega_0). \tag{57}$$

Note from (52) that $\overline{f^2(t)} = \int_{-\infty}^{\infty}M(\omega)\,d\omega = 2\int_0^{\infty}M(\omega)\,d\omega,$

so that

$$\int_0^{\infty}S(\omega)\,d\omega = j^2\tfrac{1}{2}a^2\Delta\omega\overline{f^2(t)}. \tag{58}$$

This is a useful result in that it gives the total area under the S *vs.* ω curve, which in practice may need closure. Note also that

$$\overline{\omega^2} = \int_0^{\infty}\omega^2M(\omega)\,d\omega\Big/\int_0^{\infty}M(\omega)\,d\omega. \tag{59}$$

However, the component frequencies in $f(t)$ result from the motion of an intensity pattern past the grating, and if the time for the pattern to move past one grating period is small compared with the (Lagrangian) time scale of the turbulent motions, the moving intensity pattern can be regarded as rigid in time, so that $\omega = uk_0$, where u is the component of velocity normal to the lines

of the grating, and k_0 is the grating wave-number. Therefore, using (57) and (59),

$$\overline{u^2} = \overline{\omega^2 k_0^{-2}}$$

$$= k_0^{-2} \int_0^\infty \omega^2 S(\omega)\, d\omega \Big/ \int_0^\infty S(\omega)\, d\omega. \tag{60}$$

This thus provides a method of finding the mean-square (total) velocity of the turbulent motions within the aperture. Also, $M(\omega)$, measured via $S(\omega)$ and equation (57), represents the velocity distribution (in the sense of probability of occurrence) within the aperture if ω is written as uk_0. The method does not distinguish between positive and negative velocities.

A similar method for measuring velocity fields by a frequency analysis of the light transmitted by a grating is presented theoretically by Block & Milgram (1967). They isolate a plane in the flow by passing the light radiated by the flow through a finite single lens, the degree of isolation increasing with the size of lens aperture. The 'focused' image then falls on the grating. As with the above method the application to turbulence is restricted to slowly varying flows by the condition that the time scale must be large. If one attempts to use this method to measure local velocities by using a small aperture, resolution along the optical axis is lost, and the laser Doppler velocimeter may give more meaningful results.

5. Experimental use of the single-beam configuration

5.1. *The turbulent region investigated*

To test the above theoretical ideas, a single-beam configuration was set up to investigate the refractive index structure of a rectangular tank of water, heated from below and cooled from above. This is a particularly simple way of providing a turbulent refractive index field. Also, this is not an easy situation to investigate by hot-wire anemometers as the working fluid is a liquid, with no mean velocity. The Rayleigh number was $4{\cdot}1 \times 10^8$, so the flow could be considered fully turbulent (Malkus 1954*a*).

5.2. *The optical apparatus*

Basically, the apparatus was a suitably-equipped optical bench, approximately 7 ft. long, of maximum rigidity. It had two parallel tubes on which projector and analysis subassemblies could slide. The tank was mounted on an independent support approximately half-way along the tubes. Working to maximum simplicity, the parallel beam of light was provided, on the projector subassembly, by a 24 V, 150 VA halogen-quartz lamp, pinhole and lens arrangement as indicated in figure 2. The consequences of using white light will be discussed later. The method could well be adapted to incorporate a laser beam. The parallel beam had an angular divergence better than 1 part in 2000, and the limit of resolution at the receiving grating due to finite pinhole size was 0·2 mm.

The tank, of base 33×33 cm and height 16·5 cm was constructed from optical quality plate glass, and had its conducting base heated by 8 small heater

elements clamped to its underside. The upper conducting plate was cooled by a series of water-carrying tubes, separated from the plate by a thermal resistance to ensure uniformity of temperature. Lateral temperature variation over both plates was of order $\pm 0{\cdot}2\,^{\circ}\mathrm{C}$ for a temperature difference between the plates of $5\,^{\circ}\mathrm{C}$. Temperature measurement was by surface thermocouples.

After leaving the turbulent region (the tank), the beam travelled 61·8 cm before projecting its shadowgraph image onto the grating, mounted directly on the receiving lens and capable of rotating through 360°. Turbulence in the interposed air produced a negligible signal. The gratings were of square wave transmissivity (alternate black and transparent stripes) made photographically from a large hand-painted master. Periodicity varied from 40·5 mm to 0·57 mm over 14 gratings. Three circular apertures were used, of diameters 7·30, 4·45, 3·20 cm, set by an iris in the projecting lens, but these were stopped down to 6·85, 3·95, 2·70 cm respectively at the grating to eliminate the Fresnel diffraction pattern of the iris aperture (Roe 1968). The limit of resolution set by diffraction was of order 10^{-2} mm, i.e. much less than that set by finite pinhole size. The receiving lens focussed the light transmitted by the grating onto a photocell. The latter was an OCP 71 phototransistor. Time prevented the development of a more sensitive photocell arrangement.

The three fundamental difficulties experienced all resulted from the sensitivity of detection needed, as the desired signal fluctuations were only of order 1 % of the beam signal. Even the latter was feeble as produced by the simple pinhole system. The difficulties were: (i) A poor signal/noise ratio from the photocell. For correction purposes, it was necessary to find the noise level as a function of time. (ii) Bench rigidity. Nothing short of a thick concrete floor prevented extraneous vibration contributing to the signal fluctuations. (iii) Obtaining a stable light output from the projector. Any ripple in the light output readily swamped the desired signal. The final solution was a 24 V d.c. supply from two heavy duty accumulators, with output calibrated against discharge time.

5.3. *The electronic apparatus*

The analysis of the photocell output, after removal of the d.c. signal and after amplification, took two forms: (i) The formation of a mean-square signal, for measurement of the s.d.f. of the refractive index field. (ii) The frequency analysis of the signal for measurement of velocity distributions.

(i) Squaring by vacuo-junction was tried, but the low-frequency components of the signal (which was predominantly in the range 0·5–10 Hz) meant that the junction was not working under constant filament temperature conditions. Also, the signal was characterized by periodic bursts of intensity, giving a very short life to the sensitive filament of the vacuo-junction.

The final method used was to construct a multiplier unit based on a Hall-effect multiplier device. Such devices have limitations at high frequencies, but are eminently suitable for low-frequency applications such as this. With a common signal to the two multiplier inputs, the result is the desired squared signal (Roe & Yates 1968). For averaging, because of the long averaging times needed, an integrating voltmeter comprising a voltage-frequency converter (using the

discharge characteristics of a unijunction transistor) and a decade counter was developed (Roe & Yates 1968).

(ii) Here, the photocell output was multiplied by a signal of frequency ω_0 from a U.L.F. signal generator, the multiplying again being done by a Hall-effect device. For each component frequency ω in the photocell signal, the multiplier output contained the sum and difference frequencies $\omega+\omega_0$ and $\omega-\omega_0$. Passing this (after amplification) through a low-pass active filter network (bandwidth 0·14 Hz) produced an output only when $\omega-\omega_0$ was close to zero, i.e. ω close to ω_0, the sum frequency being rejected by the filter. This low-frequency filter output was recorded on a chart recorder and the mean-square output found numerically. Zero drifts in the d.c. coupling prevented the Hall-effect squaring unit being used in this instance. (See full theory §4.2.)

6. The power spectrum results

6.1. *Treatment of results*

With time scales of order several seconds, and bursts of intensity approximately every 30 sec, time averages over less than 5 min were of little value. In practice, 1 min decade counts were integrated over 20 min, enabling a mean 1 min count and standard deviation to be calculated. These counts were corrected for noise, variations in overall transmissivity between the gratings, and the fall of battery voltage with time. The final graphs of spectral density function were harmonically corrected for the square wave grating transmissivity (see §2.6).

6.2. *The scope of the results*

The central axis of the beam was confined to the vertical central plane of the tank, at two heights, 2·7 cm and 5·9 cm above the tank base. At each height $G(k_0, 0, 0)$ and $G(0, k_0, 0)$ were measured, where the beam direction defined the z axis. At the lower beam height, the 6·85 cm aperture could not be used. Otherwise, the largest aperture available for the grating of choice was used (the high wave-number gratings were of restricted aperture due to the photographic method of construction).

6.3. *The function E*

This function, given by equation (32), was calculated on the basis of the mean wavelength of the white light used, and is shown as a log-log plot in figure 6. It will be noted that E deviates from a fourth-power dependence on k_0 only at the high wave-number end of the grating range used. From §2.5 it may thus be deduced that the wavelength of the light used only becomes important at these high wave-numbers. Any adverse effects of using white instead of monochromatic light can only be expected therefore for $\log_{10}(k_0) \gtrsim 1{\cdot}8$.

6.4. *Graphical presentation*

Recalling equation (31), $\overline{\Delta J^2} = (4\pi^3 I_0^2 \beta^2 \lambda^2 L^2) N^3 E G$.

Figures 7 and 8 show respectively $\overline{\Delta J^2}$ *vs.* wave-number, and G *vs.* wave-number, G being calculated from the above relation. k_0 is 2π/(grating wavelength), and

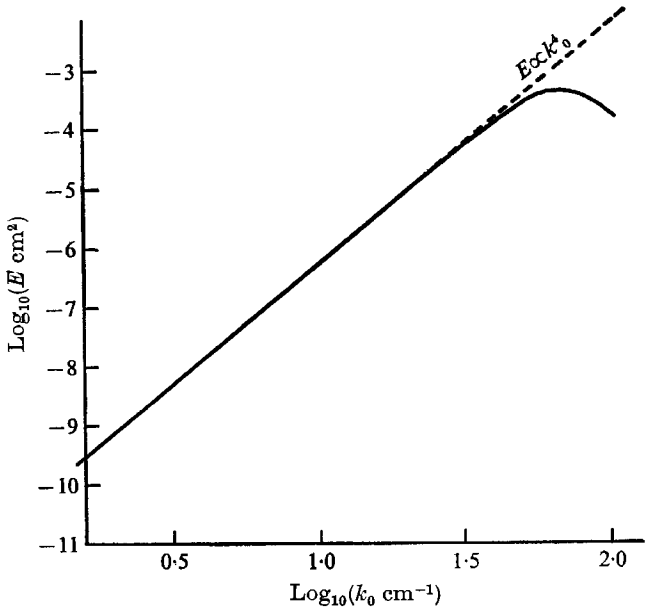

FIGURE 6. The function $E(k_0^2/N, z, H)$: $N = 1{\cdot}3 \times 10^5\ \mathrm{cm}^{-1}$, $z = 61{\cdot}8$ cm, $H = 33{\cdot}0$ cm.

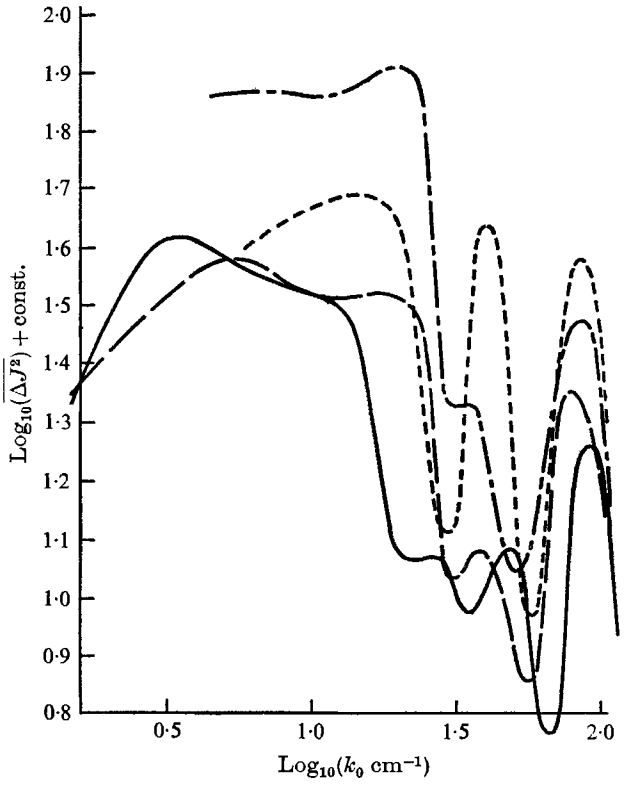

FIGURE 7. Mean square signal fluctuation. ——, upper height, vertical distribution, (grating lines horizontal); — —, upper height, horizontal distribution (grating lines horizontal); - - - -, lower height, vertical distribution; — · —, lower height, horizontal distribution.

measured in cm^{-1}. Although figure 8 is the principal result here, figure 7 is useful in showing the finer structure of the spectrum because of the relatively weak dependence of $\overline{\Delta J^2}$ upon k_0. For clarity, points have been omitted from the curves, but each curve was constructed from approximately 20 points, each with an experimental tolerance of about $\pm 0{\cdot}04$ in both $\log_{10}(\overline{\Delta J^2})$ and $\log_{10}(G)$.

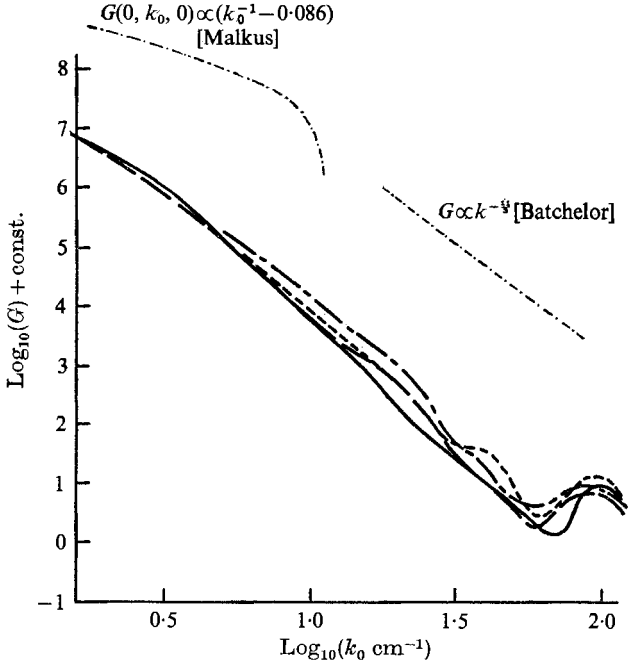

FIGURE 8. Spectral density function. ——, upper height, $G(0, k_0, 0)$, vertical distribution; — —, upper height, $G(k_0, 0, 0)$, horizontal distribution; - - - -, lower height, $G(0, k_0, 0)$, vertical distribution; — - —, lower height, $G(k_0, 0, 0)$, horizontal distribution; —·—·—, theoretical curves.

7. Discussion of the spectral density function results

7.1. *The nature of the signal*

Periodic surges in signal strength, corresponding to surges in turbulent activity, were observed fairly regularly on a time scale of order 30 sec. These surges were emphasized by the squaring operation. Their precise origin did not become known during these investigations, but familiarity with their characteristics led to some intuitive ideas.

Generally, the longer the quiescent period prior to a surge, the more intense was the ensuing surge. Frequently, indeed, no distinct peak would occur for several 'cycles', but the signal level would be higher than the aforementioned quiescent periods, as if the surges had become broken into smaller, more frequent units. It seemed that over a period of about 30 sec, a certain amount of energy had to be released in the tank by the creation of turbulent motions and subsequent dissipation (corresponding to the net heat input over that period). This energy was sometimes released quasi-continuously, sometimes in surges.

In the latter case, energy was stored in the conduction layer (approximately 1 mm thick in this instance) adjacent to the hot tank base until the situation became unstable, when a burst of hot-water plumes would rise from the conduction layer until the stored energy was released. Another quiescent period would then follow. Whether the creation of turbulent energy took place quasi-continuously, or in surges, probably depended upon how the flow field adjacent to the conduction layer affected the stability of this layer.

7.2. *The presence of the tank side-walls*

Townsend (1959) has shown in an air-box experiment that the convective motions are determined primarily by the motion and structure of the lower conduction layer, which here is too thin to be affected appreciably by external influences at such relatively large distances from the centre as the side-walls. This is not likely to be the case during quiescent periods, but the signals are much smaller then. However, for the width: height ratio of 2:1 used here (determined mainly by practical optical considerations) it would perhaps be too optimistic to assume that turbulent activity, particularly for large-scale motions, was a function of height above the tank base only, as is assumed in most theoretical models.

7.3. *Theoretical forms for the spectral density function* $G(l, m, n)$

It will here be assumed that $G(l, m, n)$ the s.d.f. for refractive index fluctuations, is proportional to the s.d.f. for temperature fluctuations, as indicated in §2.4.

Malkus (1954*b*) considers a simple model of convective heat transfer, in which the instantaneous temperature fluctuation θ is taken as a function of height in the tank (y) only. He shows that for a total height d

$$G(0, m, 0) \propto \left(\frac{md}{\pi}\right)^{-1}\left(1-\frac{md/\pi}{p_0+1}\right), \tag{61}$$

where θ is written in the form $\sum_{p=1}^{p_0} f(p)\sin(p\pi y/d)$, $m = p\pi/d$, and p_0 is the highest mode with significant contribution to $\overline{\theta^2}$. In this case p_0 was calculated as approximately 60, so

$$G(0, m, 0) \propto m^{-1}\left(1-\frac{md/\pi}{61}\right) = m^{-1} - 0{\cdot}086.$$

This is plotted, with a vertical shift for clarity, in figure 8. This model is only applicable to the small wave-number end of the spectrum, and within this range agreement of slope with the experimental curve for $G(0, m, 0)$ is fair.

Note that the experimental method presented does not account for constants of proportionality (i.e. absolute calibration of the apparatus), leaving the experimental log-log plots arbitrary to the extent of an ordinate constant. The aim of the investigation was merely to find slopes of these log-log plots. A method of obtaining absolute calibration is given by Roe (1968).

The large wave-number end of the spectrum is discussed by Batchelor (1959*b*) in a paper on the small-scale variation of convected scalar quantities like temperature. The scale is assumed sufficiently small for the temperature fluctuations

to be regarded as passive quantities on which is imposed a velocity field, which may or may not be due to (large-scale) temperature variation. The treatment is analogous to the Kolmogoroff (1941) theory of velocity fields. The theory relies on the existence of an equilibrium range of wave-numbers, within which there may be a 'convective subrange' (analogous to the Kolmogoroff 'inertial subrange') if the turbulent Reynolds number is high enough.

Isotropy is assumed for the equilibrium range. Just as velocity fields tend to isotropy at high wave-numbers, so, it is assumed, do temperature fields. Thus $G(l, m, n)$ becomes $G(K)$ as in (30).

For the convective subrange, Batchelor shows that

$$G(K) \propto \epsilon_\theta \epsilon^{-\frac{1}{3}} K^{-\frac{11}{3}}, \tag{62}$$

where ϵ_θ is the contribution to $-(\partial/\partial t)$ ($\frac{1}{2}$ mean square temperature fluctuation $\overline{\theta^2}$) from conduction, and ϵ is the contribution to $-(\partial/\partial t)$ ($\frac{1}{2}$ mean square velocity fluctuation $\overline{u^2}$) from viscous dissipation.

Alternatively, the spectral contribution to $\overline{\theta^2}$ between K and $K+dK$ is $4\pi K^2 G(K)\,dK$, where

$$4\pi K^2 G(K) \propto K^{-\frac{5}{3}} \tag{63}$$

This is analogous to the much-investigated $-\frac{5}{3}$ power law in velocity fields.

The function $G(K) \propto K^{-\frac{11}{3}}$ is shown in figure 8 (with a vertical shift for clarity), and the agreement with the present experimental results is seen to be very good over a significant range of wave-numbers.

It was estimated, from time and velocity scales, that the turbulent Reynolds number $R_\epsilon(\lambda) = u\lambda/\nu$ (where λ is the Taylor dissipation scale) was here of order 40. Batchelor (1959*a*) shows that an equilibrium range exists when $R_\epsilon \gtrsim 50$, so a small one may exist here, but the existence of a convective subrange seems unlikely. The above agreement with theory is thus a little surprising, although a $-\frac{5}{3}$ power law has been observed in velocity fields with a turbulent Reynolds number too small for an inertial subrange to exist. Also, these $-\frac{5}{3}$ power laws do not seem to depend critically on having perfect isotropy.

Batchelor (1959*b*) suggests that for the case $\nu \gg \kappa$ (as for water), the viscous cut-off of the spectrum occurs at a wave-number of order $(\epsilon/\nu^3)^{\frac{1}{4}}$, and the conduction cut-off at $(\epsilon/\nu\kappa^2)^{\frac{1}{4}}$, the ratio being the Prandtl number (ν/κ) raised to power $\frac{1}{2}$. This is approximately 2·5 for water at 25 °C, as here. Also, in between the cut-offs, the spectral density function takes the form

$$G(K) \propto K^{-3} \exp[\kappa K^2/\gamma], \tag{64}$$

where γ (negative) is the average least principal rate of strain on the high wave-number components of $\overline{\theta^2}$ due to the convective motions of the velocity field with wave-numbers $\lesssim (\epsilon/\nu^3)^{\frac{1}{4}}$.

Figure 8 does indeed show two apparent cut-offs, at $\log_{10} k_0 \simeq 1{\cdot}75$ and $\log_{10} k_0 \simeq 2{\cdot}15$, i.e. $k_0 = 55$ and $140\,\mathrm{cm}^{-1}$ respectively. This is a ratio of 2·5 as predicted. There is also a change in slope between these two cut-offs, but the increase in slope is far too large, most probably due to the function E being

too small at these wave-numbers. It will be recalled (§6.3) that E as used here is unreliable for $\log_{10}(k_0) \gtrsim 1{\cdot}8$, because of the use of white, instead of monochromatic, light.

7.4. *Additional observed features of the spectral density function* $G(l, m, n)$

(i) If it is assumed that the peak in the s.d.f. curves for $1{\cdot}75 < \log_{10}(k_0) < 2{\cdot}15$ is explained as above, it still remains to explain the undulations for $\log_{10}(k_0) < 1{\cdot}75$, particularly the rise and sharp fall (figure 7) at $\log_{10}(k_0) \simeq 1{\cdot}4$ (wavelength 2·5 mm). It is apparent that some significant structure exists at this wavelength. One advantage of an optical method is that a screen can be interposed and the structure observed.

This wavelength was found to correspond to the width of the interfacial region between the plumes of hot fluid and the surrounding cooler fluid. The width of this region is governed by combined molecular and turbulent diffusion.

Similar, but unexplained, undulations have been observed by Deardorff & Willis (1967), but at a smaller relative wave-number (wavelength expressed as a fraction of tank height). They towed hot wires through a heated air-box, and obtained the s.d.f. in the range $10d$ to $\frac{1}{5}d$, whereas the present optical method was complementary in the sense that it covered the range $\frac{1}{4}d$ to $\frac{1}{320}d$. Their tank width:height ratio was variable in the range 25:1 to 3:1, whereas the present tank was fixed at 2:1. This could explain why their undulations were at a smaller wave-number, as reduction of this ratio pushes energy to smaller relative wavelengths, i.e. higher relative wave-numbers.

(ii) The s.d.f. curves corresponding to the beam at the lower height lie above those for the beam at the upper height (the arbitrary ordinate constant was the same for all curves). This implies that, for the range of wave-numbers covered, the contribution to $\overline{\theta^2}$ is greatest near to the tank base. This is to be expected, as it is in this region that a large proportion of the turbulent fluctuations are generated.

(iii) It will be observed that, for a given beam height, the s.d.f. curves have similar shape, but with a relative shift parallel to the wave-number axis. This is best seen in figure 7. This fact can be used to estimate the extent of anisotropy in the turbulent field.

For the upper beam height case, this shift corresponds to an 'eddy' height-width ratio of about 1·6:1 for $\log_{10}(k_0) < 1{\cdot}5$, with the extent of anisotropy decreasing to zero with increasing wave-number. The tendency of turbulent fields to isotropy at high wave-numbers ('local isotropy') is an integral part of turbulence theory, and its existence is thus demonstrated here (see also §7.3).

The extent of anisotropy is less at the lower height (vertical elongation presumably being restricted by the proximity of the tank base), the height:width ratio being about 1·2:1 for $\log_{10}(k_0) < 1{\cdot}5$, again decreasing to unity with increasing wave-number.

(iv) Note also that, comparing upper and lower beam height results, more energy is pushed into the smaller scale structure, at the expense of larger scales, as the tank base is approached.

8. The velocity distribution results

8.1. *The results*

Results were taken only at the lower beam height, with the lines of the 1·45 mm grating horizontal (to measure vertical motions) and vertical (to measure horizontal motions). The frequency distribution in the signal for these two cases is shown in figures 9 and 10.

Because of the finite bandwidth of the filter, it was unreasonable to analyze below 1 Hz, as below this frequency the filter passed a proportion of the sum frequency, in addition to the desired difference frequency (see §4.2). Closure below 1 Hz was effected by using (58), and is shown dashed in figures 9 and 10.

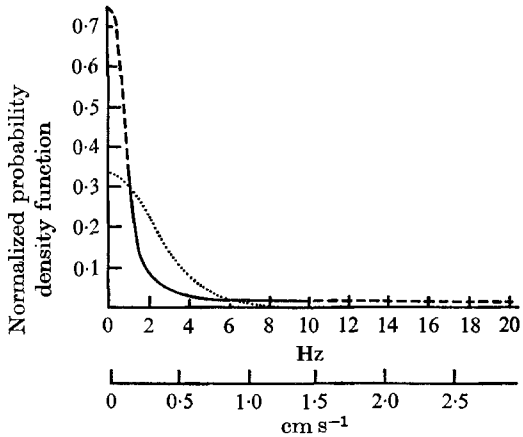

FIGURE 9. Velocity distribution within the beam aperture: vertical motions.

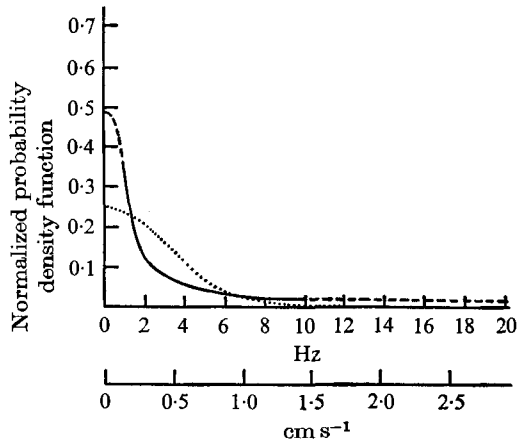

FIGURE 10. Velocity distribution with the beam aperture: horizontal motions.

8.2. *Comments on the results*

The principal difficulty experienced in this method was the noise output from the photocell, which gave an extended tail to the frequency distributions. It was considered that above 10 Hz the signal was largely noise, and so for calculating

the r.m.s. velocity the curve was cut off here (it is shown dashed beyond this point). This rather arbitrary approach was used as only an estimate of the r.m.s. velocity was required. Using (60), the r.m.s. velocity for vertical motions was 0·35 cm/s, and 0·46 cm/s for horizontal motions.

Also shown (dotted lines) in figures 9 and 10 are Gaussian distributions having the same variance as the experimental distributions. It will be observed that the observed distributions have a much higher flatness than the corresponding Gaussian distributions. This might be expected of a motion which by nature is spasmodic, with small velocities in quiescent periods, and large velocities when a plume passes through the beam. This flatness is probably exaggerated by the fact that motions associated with the plumes contain the largest temperature and refractive index fluctuations. In addition, the flatness is greater for vertical than for horizontal motions. This is because vertical motions are more dominated by the spasmodic passing of plumes.

9. Statistical analysis of the spectral density function results

9.1. *The information available*

It became apparent during the course of this investigation that the statistical distribution of the 1 min signals contained information about the Eulerian time-scale of events within the beam aperture. The following analysis was used to extract this information.

9.2. *Preliminary analysis*

Let w be the direct signal (fluctuation), i.e. $\overline{w} = 0$. Let x be the squared signal, i.e. $x = w^2$. Also, let the probability of the direct signal lying between w and $w+dw$ be $p(w)dw$. So, if the probability of the squared signal lying between x and $x+dx$ is $P(x)dx$,

$$P(x)dx = P(w^2)d(w^2) = p(w)dw + p(-w)dw = 2p(w)dw$$
$$= \frac{p(w)d(w^2)}{|w|}, \quad \text{i.e. } P(x) = \frac{p(w)}{|w|}. \tag{65}$$

This assumes $p(w)$ is symmetrical about $w = 0$. $P(x)$ is therefore weighted towards low values of $|w|$, i.e. low values of x.

The direct signal results from a summation of events over the path length of the beam through the turbulence, a high proportion of which are uncorrelated. It is not an unreasonable approximation therefore to take $p(w)$ as a normal distribution, viz.

$$p(w) = \frac{1}{\sqrt{(2\pi)w_0}} \exp\left[-\frac{1}{2}\frac{w^2}{w_0^2}\right]. \tag{66}$$

Then

$$\overline{x} = \int_0^\infty xP(x)dx = w_0^2,$$

and the probability of the squared signal lying below the mean, $\overline{x}$, is

$$\int_0^{\overline{x}} P(x)dx = \frac{1}{\sqrt{(2\pi)w_0}} \int_0^{w_0} x^{-\frac{1}{2}} \exp\left[-\frac{1}{2}\frac{x}{w_0^2}\right]dx = 0{\cdot}68. \tag{67}$$

Now if the sampling, i.e. integrating, time of 1 min is much less than the Eulerian integral time-scale $\mathscr{T}$ of events contributing to the signal, the 1 min readings should have the above $P(x)$ distribution, with a proportion 0·68 below the mean. But if the sampling time is much larger than $\mathscr{T}$, the original nature of the direct signal will be lost, and the squared signal will become effectively a random array of uncorrelated pulses, having a normal distribution, the 1 min readings then having a proportion 0·5 below the mean. For 735 1 min readings, a proportion 0·56 were on average below the 20 min mean. It was expected therefore that $\mathscr{T}$ was within the 1 min sampling time.

9.3. *Calculation of the integral time-scale* $\mathscr{T}$

$x(t)$ is the instantaneous squared signal. Let x_1 be the 1 min sample, i.e.

$$x_1 = \frac{1}{T}\int_0^T x(t)\,dt, \quad \text{with} \quad T = 1\,\text{min}. \tag{68}$$

Now
$$x_1 = \bar{x} + e_1, \text{ so } \overline{x_1^2} = \overline{(\bar{x}+e_1)^2} = \bar{x}^2 + \overline{e_1^2} = \bar{x}^2 + \sigma^2, \tag{69}$$

where
$$\bar{x} = \bar{x}_1 = \text{average of } x(t) \text{ over all time (20 min here)},$$
$$e(t) = \text{instantaneous deviation of } x(t) \text{ from } \bar{x},$$
$$e_1 = \text{deviation in 1 min sample},$$
$$\sigma = \text{standard deviation in 1 min sample}.$$

From (68),
$$\overline{x_1^2} = \overline{\left[\frac{1}{T}\int_0^T x(t)\,dt\right]^2} = \frac{1}{T^2}\int_0^T\int_0^T \overline{[\bar{x}+e(t)][\bar{x}+e(t')]}\,dt\,dt'$$
$$= \bar{x}^2 + \frac{1}{T^2}\int_0^T\int_0^T \overline{e(t)\,e(t')}\,dt\,dt',$$

so from (69),
$$\sigma^2 = \frac{1}{T^2}\int_0^T\int_0^T \overline{e(t)\,e(t')}\,dt\,dt'. \tag{70}$$

Transforming this integral,

$$\sigma^2 = \frac{2}{T^2}\int_0^T dt\int_0^t \overline{e(t)\,e(t')}\,dt' = \frac{2}{T^2}\int_0^T dt\int_0^t \overline{e(t)\,e(t-\tau)}\,d\tau$$
$$= \frac{2}{T^2}\int_0^T dt\int_0^t R(\tau)\,d\tau, \tag{71}$$

where $\tau = t'-t$, and $R(\tau)$ is the time correlation function for fluctuations in $x(t)$. Therefore

$$\sigma^2 = \frac{2}{T^2}\left[t\int_0^t R(\tau)\,d\tau\right]_0^T - \frac{2}{T^2}\int_0^T tR(t)\,dt$$
$$= \frac{2}{T^2}\int_0^T (T-\tau)R(\tau)\,d\tau. \tag{72}$$

If $R(\tau) \ll 1$ for $\tau > T$, i.e. for time-scales less than T, as here,

$$\sigma^2 = \frac{2}{T}\int_0^T R(\tau)\,d\tau \simeq \frac{2}{T}\int_0^\infty R(\tau)\,d\tau. \tag{73}$$

Therefore
$$\frac{\sigma^2}{\overline{e^2(t)}} = \frac{2}{T}\int_0^\infty \frac{R(\tau)\,d\tau}{\overline{e^2(t)}} = \frac{2}{T}\mathscr{T} \tag{74}$$

by definition of integral time-scale (Hinze 1959). Now $\overline{e^2(t)} = \overline{w^4} - w_0^4$, and if a normal distribution is again assumed for $p(w)$, $\overline{w^4} = 3w_0^4$, giving $\overline{e^2(t)} = 2w_0^4 = 2\bar{x}^2$.

Hence, from (74),
$$\left[\frac{\sigma}{\bar{x}}\right]^2 = \frac{4}{T}\mathscr{T}. \tag{75}$$

This simple relation enables $\mathscr{T}$ to be calculated from values of $\sigma/\bar{x}$ extracted from the experimental results.

9.4. *An alternative approach*

As above, assume a normal distribution for the direct signal $w(t)$. Then, from (65) and (66),
$$P(x) = \frac{1}{\sqrt{(2\pi)w_0}}x^{-\frac{1}{2}}\exp\left[-\frac{x}{2w_0^2}\right]. \tag{76}$$

Suppose now that x is constant for time intervals of length τ_0, then change to an uncorrelated value for period τ_0 (i.e. as the number of steps $\to\infty$, $\tau_0 \to \mathscr{T}$, the required time-scale).

Define
$$v = \frac{1}{\tau_0}\int_0^{2\tau} x(t)\,dt, \tag{77}$$

the integrated squared signal over $2\tau_0$, divided by τ_0.

For the first two intervals (see figure 11), $v = x' + x''$, so x' has the range 0 to v.

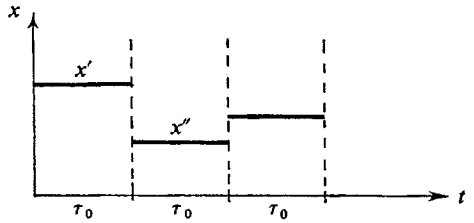

FIGURE 11. Statistical model for squared signal.

Thus the probability density function for v, over two periods τ_0, is
$$P_2(v) = \int_0^v P(x')P(v-x')\,dx' \tag{78}$$
$$= \frac{1}{2w_0^2}\exp\left[-\frac{v}{2w_0^2}\right]. \tag{79}$$

In similar fashion, the probability density function for
$$v = \frac{1}{\tau_0}\int_0^{4\tau_0} x(t)\,dt,$$

the integration now being over $4\tau_0$, can be found, viz.

$$P_4(v) = \int_0^v P_2(x'+x'')\,P_2[v-(x'+x'')]\,d(x'+x'$$

$$= \left(\frac{1}{2w_0^2}\right)^2 v \exp\left[-\frac{v}{2w_0^2}\right]. \tag{80}$$

Similarly,
$$P_6(v) = \int_0^v P_2(x'+x'')\,P_4[v-(x'+x'')]\,d(x'+x'')$$

$$= \left(\frac{1}{2w_0^2}\right)^3 \frac{v^2}{2!} \exp\left[-\frac{v}{2w_0^2}\right]. \tag{81}$$

By induction,
$$P_n(v) = (2w_0^2)^{-\frac{1}{2}n} \frac{v^{\frac{1}{2}n-1}}{(\frac{1}{2}n-1)!} \exp\left[-\frac{v}{2w_0^2}\right]. \tag{82}$$

$P_n(v)dv$ is the probability that, after n steps, the integrated squared signal lies between v and $v+dv$ (n even).

The average value of this integrated signal after n steps is (using (82))

$$\bar{v}(n) = \int_0^\infty v P_n(v)\,dv = nw_0^2.$$

It is easily verified by differentiation that $P_n(v)$ has its maximum value at $v(n) = (n-2)w_0^2$. Thus the most probable v is less than the mean v, the relative difference diminishing as n increases; this is the conclusion reached by a different method in §9.2.

From (82) can be calculated the proportion of 1 min samples, B, lying below the mean (i.e. the probability of the 1 min integrated squared signal lying below the mean).

This is
$$B = \int_0^{nw_0^2} P_n(v)\,dv = \frac{2^{-b}}{(b-1)!}\int_0^{2b} z^{b-1}e^{-\frac{1}{2}z}dz \quad \text{with} \quad b = \tfrac{1}{2}n.$$

After some reduction, this gives

$$B = 1 - e^{-b}Z(b), \tag{83}$$

where
$$Z(b) = 1 + \frac{b}{1!} + \frac{b^2}{2!} + \ldots + \frac{b^{b-1}}{(b-1)!}, \tag{84}$$

a truncated e^b series. The table below shows B evaluated.

$b = \frac{1}{2}n$	1	2	3	4	5
B	0·6321	0·5941	0·5779	0·5665	0·5596
$b = \frac{1}{2}n$	6	7	8	9	10
B	0·5538	0·5506	0·5478	0·5443	0·5422

Note the slow convergence to 0·5. Knowing the proportion of 1 min samples lying below the mean, this table enables the number of time-scale steps, n, in the 1 min interval to be found—hence the time-scale.

9.5. *The values of the time-scale found*

For the method of § 9.3, the following results were obtained for the time-scale $\mathscr{T}$ in seconds.

Aperture (cm)	Vertical motions beam upper height	Hor. motions upper height	Vert. motions lower height	Hor. motions lower height
6·85	$0{\cdot}90 \pm 0{\cdot}10$	$1{\cdot}45 \pm 0{\cdot}10$	–	–
3·95	$1{\cdot}95 \pm 0{\cdot}40$	$2{\cdot}65 \pm 0{\cdot}35$	$1{\cdot}75 \pm 0{\cdot}60$	$2{\cdot}40 \pm 0{\cdot}70$
2·70	$2{\cdot}65 \pm 0{\cdot}40$	$2{\cdot}80 \pm 0{\cdot}25$	$3{\cdot}05 \pm 0{\cdot}55$	$2{\cdot}65 \pm 0{\cdot}25$

The following conclusions may be drawn within experimental error: (i) No detectable difference in upper and lower height time-scales. (ii) No detectable difference for horizontal and vertical motions. (iii) A distinct trend towards longer time-scales for smaller apertures. This is due to a smaller aperture giving more localized measurements, with less opportunity for events to average themselves within the area of the aperture. This idea can be extended further, for extrapolating the above time-scales to zero aperture gives the Eulerian time-scale at a point, $\mathscr{T}_p$ say. For vertical motions $\mathscr{T}_p = 4{\cdot}0 \pm 0{\cdot}5$ sec. For horizontal motions $\mathscr{T}_p = 3{\cdot}7 \pm 0{\cdot}2$ sec.

The corresponding results for the method of § 9.4 did not show the above trends as clearly, due to the combination of random experimental error and the slow convergence of the function B. A mean value for all configurations was thus found. An average of 90 values gave $B = 0{\cdot}548 \pm 0{\cdot}008$, and n (from the table) as 16 ± 6. The corresponding time-scale of $60/n$ was therefore $4{\cdot}3 \pm 1{\cdot}6$ sec.

It is reassuring that these two quite different methods give consistent results.

REFERENCES

Batchelor, G. K. 1957 Wave scattering due to turbulence. *Symp. on Naval Hydrodynamics*. No. 515, Nat. Acad. Sci.

Batchelor, G. K. 1959*a* *The Theory of Homogeneous Turbulence*. Cambridge University Press.

Batchelor, G. K. 1959*b* The small-scale variation of convected quantities like temperature in a turbulent field. *J. Fluid Mech.* **5**, 113–133.

Block, M. J. & Milgram, H. 1967 Optical detection of local fluid-flow velocities by filtering in space and time. *J. Optical Soc. Am.* **57**, 604–609.

Deardorff, J. W. & Willis, G. E. 1967 Investigation of turbulent thermal convection between horizontal plates. *J. Fluid Mech.* **28**, 675–704.

Fisher, M. J. & Krause, F. R. 1967 The crossed beam correlation technique. *J. Fluid Mech.* **28**, 705–717.

Hinze, J. O. 1959 *Turbulence, an Introduction to its Mechanism and Theory*. McGraw-Hill.

Kolmogoroff, A. N. 1941 The local structure of turbulence in incompressible viscous fluid for very large Reynolds numbers. *Comptes rendus de l'Academie des Sciences de l'U.R.S.S.* **30**, 301–305.

Malkus, W. V. R. 1954*a* Discrete transitions in turbulent convection. *Proc. Roy. Soc.* A **225**, 185–195.

Malkus, W. V. R. 1954*b* The heat transport and spectrum of thermal turbulence. *Proc. Roy. Soc.* A **225**, 196–212.

PROTHEROE, W. M. 1964 The motion and structure of stellar shadow-band patterns. *Quart. J. Roy. Met. Soc.* **90**, 27–42.

ROE, G. E. 1968 An investigation of turbulence by wave scattering. Ph.D. thesis, University of Cambridge.

ROE, G. E. & YATES, G. G. 1968 An electronic arrangement for measuring time mean products and squares in fluid turbulence at low frequencies. *J. Sci. Instrum.* series 2, **1**, 1185–1187.

TATARSKI, V. I. 1961 *Wave Propagation in a Turbulent Medium.* McGraw-Hill.

TOWNSEND, A. A. 1959 Temperature fluctuations over a heated horizontal surface. *J. Fluid Mech.* **5**, 209–241.

TOWNSEND, A. A. 1965 The interpretation of stellar shadow-bands as a consequence of turbulent mixing. *Quart. J. Roy. Met. Soc.* **91**, 1–9.